UC Santa Barbara
UC Santa Barbara Previously Published Works

Title

Reliability of InAsGaAs Quantum Dot Lasers Epitaxially Grown on Silicon

Authors

Liu, Alan Y
Herrick, Robert W
Ueda, Osamu
et al.

Fluctuation and commensurability effect of exciton density wave

Sen Yang,[1] L. V. Butov,[1] B. D. Simons,[2] K. L. Campman,[3] and A. C. Gossard[3]

[1]*Department of Physics, University of California at San Diego, La Jolla, California 92093-0319, USA*
[2]*Cavendish Laboratory, Madingley Road, Cambridge CB3 0HE, United Kingdom*
[3]*Materials Department, University of California at Santa Barbara, Santa Barbara, California 93106-5050, USA*

At low temperatures, indirect excitons formed at the in-plane electron-hole interface in a coupled-quantum-well structure undergo a spontaneous transition into a spatially modulated state. We report on the control of the instability wavelength, measurement of the dynamics of the exciton emission pattern, and observation of the fluctuation and commensurability effect of the exciton density wave. We found that fluctuations are suppressed when the instability wavelength is commensurate with defect separation along the exciton density wave. The commensurability effect is also found in numerical simulations within the model describing the exciton density wave in terms of an instability due to stimulated processes.

I. INTRODUCTION

An indirect exciton (IX) is a bound pair of an electron and a hole in separated quantum-well layers [1,2]. Long lifetimes allow IXs to cool down below the temperature of quantum degeneracy, giving an opportunity to study low-temperature exciton states. Remarkable phenomena in cold IXs including a spontaneous transition into a spatially modulated exciton state [3,4], spontaneous coherence and condensation of excitons [4–6], perfect Coulomb drag [7], long-range spin currents and spin textures [4,8], enhanced exciton radiative recombination [9], tunneling recombination [10,11], and scattering [12] rates, and correlation phenomena [13–19] have been found.

A spatially ordered excitonic state was observed in which exciton density undergoes modulational instability [3]. This state, dubbed the macroscopically ordered exciton state (MOES), exhibits approximately periodic spatial modulation within an exciton ring. The MOES forms when the IX gas is cooled below a few kelvin close to the temperature of quantum degeneracy ($T_0 = 2\pi\hbar^2 n/m \simeq 3$ K for the exciton density per spin state $n = 10^{10}$ cm^{-2} and exciton mass $m = 0.22m_0$ relevant to the experiments).

The MOES occurrence initiated intensive experimental [4–6,20] and theoretical [21–28] studies. The experiments revealed the following MOES properties. (i) The exciton coherence length in the MOES reaches microns [4–6], an order of magnitude greater than in a classical exciton gas, showing that the MOES is a condensate in momentum space. (ii) The MOES forms in the external ring of the exciton pattern formation [3]. The external ring itself forms on the interface between the electron-rich and hole-rich regions [29–33]. This interface is essential for the MOES since no spontaneous density modulation is observed in another exciton ring—the inner ring where no such interface is involved [3,34,35]. (iii) The MOES is characterized by repulsive IX interaction [20]. This is consistent with the predicted repulsive interaction between IXs [36], which are dipoles with a built-in dipole moment $\sim ed$, where d is the distance between the electron and hole layers. Repulsive interaction forms a negative feedback to density fluctuation, thus acting against density modulation. A positive feedback to density fluctuation leading to spontaneous density modulation and consistent with the

measured properties of the MOES is needed to explain the MOES origin. A search for a mechanism responsible for the formation of the MOES had led to a model attributing an instability to stimulated processes of exciton formation at the interface between the electron-rich and hole-rich regions that build up near quantum degeneracy [22].

Here, we report on the observation of fluctuations of the exciton density wave and finding the commensurability effect: The fluctuations are suppressed when the number ν of wavelengths of the exciton density wave confined between defects is an integer. This phenomenon in cold exciton gases is presented in Fig. 1(c). As detailed further in the text, the suppression of fluctuations of the exciton density wave at integer ν is revealed by pronounced maxima in the standard deviation of the second-order correlation function for the IX emission intensity profile along the exciton density wave between defects. We also analyzed the stability of the exciton density wave by numerical simulations and found the commensurability effect within the model describing the exciton density wave in terms of an instability due to stimulated processes.

II. EXPERIMENT

The coupled-quantum-well (CQW) structure contains two 8 nm GaAs QWs separated by a 4 nm Al$_{0.33}$Ga$_{0.67}$As and surrounded by 200 nm Al$_{0.33}$Ga$_{0.67}$As barrier layers (for details see [3]). IXs in the CQW are formed from electrons and holes confined in the separated QWs. Photoexcitation was done by a cw 633 nm HeNe laser with a 5 μm spot. The small disorder in the CQW is indicated by the IX emission linewidth of about 1 meV in the ring. The experiments were performed at $T = 1.6$ K. IX emission images were acquired by a CCD camera after an 800 ± 5 nm interference filter matching the IX energy. The CCD recorded the evolution of the IX emission image with the repetition rate 30 frames per second.

Previous studies have shown that increasing the laser excitation power P leads to the increase of the external ring radius due to the enhancement of the hole source, while increasing the applied gate voltage V leads to the decrease of the ring radius due to the enhancement of the electron source
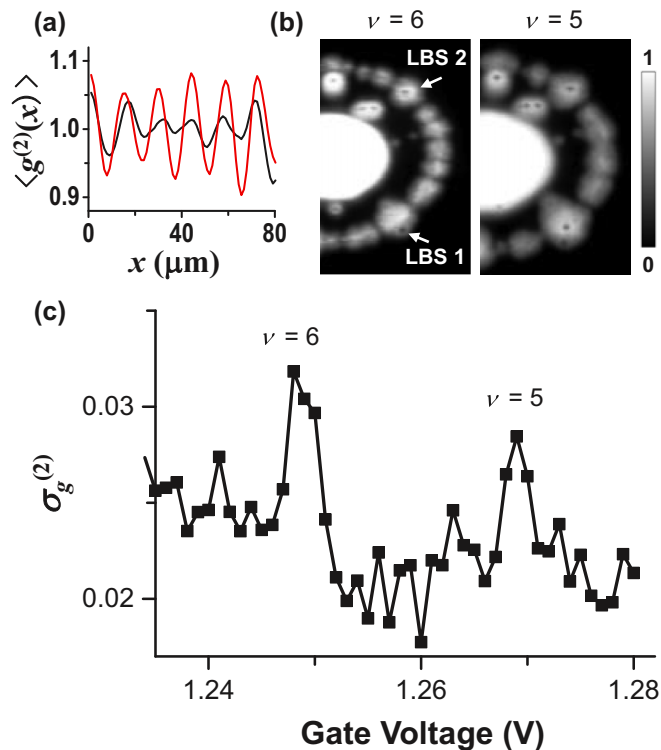
FIG. 1. (Color online) (a) The second-order correlation function $g^{(2)}$ for the IX emission intensity profile along the exciton density wave between LBS 1 and LBS 2 of length L [shown in (b)] with averaging over 800 frames in a 27 s data acquisition movie. The commensurability numbers $\nu = L/\lambda_c$ are 7 (red) and 6.5 (black). (b) Images of the IX emission pattern averaged over 800 frames for different ν. Left (right) image shows six (five) wavelengths of exciton density wave between LBS 1 and LBS 2, where LBS indicates a localized bright spot. (c) Standard deviation of $g^{(2)}$ as a function of gate voltage, which controls the instability wavelength λ_c. For all data, V and P are varied simultaneously as in Fig. 2(c) so that the ring radius is fixed. The peaks indicate the suppression of phase fluctuations of the exciton density wave at integer ν.
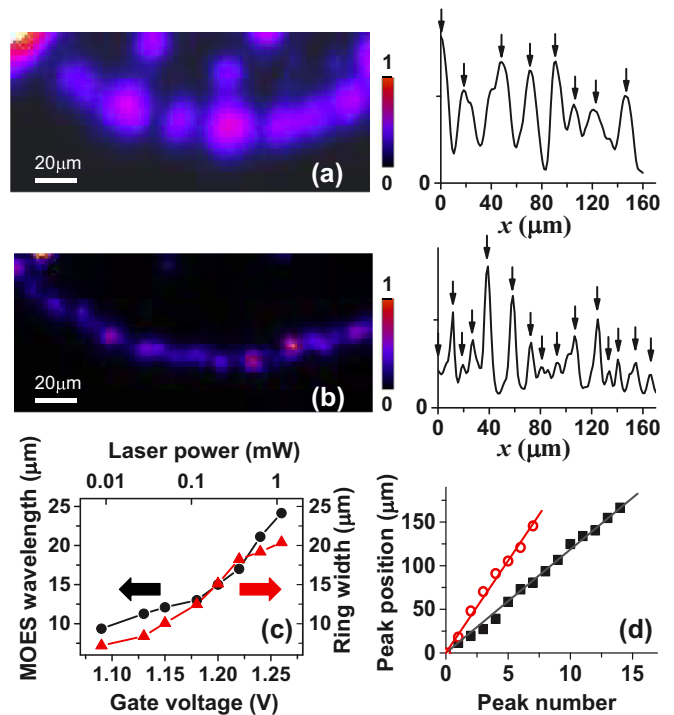

FIG. 2. (Color online) (a),(b) A segment of the external exciton ring and the corresponding IX emission intensity profile along the ring. (a) Gate voltage $V = 1.26$ V, laser excitation power $P = 1.12$ mW. (b) $V = 1.13$ V, $P = 0.028$ mW. (c) The MOES wavelength λ_c (points) and the ring width δ_r (triangles) vs V and P, which are varied simultaneously so that the ring radius is fixed. (d) The MOES bead position vs peak number for the rings shown in (a) (circles) and (b) (squares).

[29–33,35]. In this work, we vary P and V simultaneously so that the ring radius and position are kept constant. The simultaneous increase of P and V leads to the enhancement of both electron and hole sources and, as a result, exciton density in the ring. Figure 2(c) shows that increasing the exciton density leads to an increase of the MOES wavelength λ_c. MOES beads are essentially equidistant, forming an ordered array, while the bead intensities vary from bead to bead [Figs. 2(a), 2(b), and 2(d)]. We refer to such a quasiperiodic array as an excitonic density wave. λ_c is controlled by P and V within the range 9–24 μm for the experiments in Fig. 2. λ_c values up to 40 μm were achieved for other ring radii set by other values of P and V. Figure 2(c) also shows that increasing the exciton density leads to an increase of the ring width δ_r along with the increase of the MOES wavelength λ_c.

The exciton pattern formation also includes localized bright spots (LBSs), which are associated with defects in the sample—electron current filaments [29]. Figure 3 and a movie in the Supplemental Material [37] show that LBS beads are stable while MOES beads fluctuate with time. Both these

fluctuations [Figs. 3(b)–3(e)] and the λ_c variation with density for the fixed ring position [Fig. 2(c)] indicate that the exciton density modulation in the MOES forms spontaneously rather than due to the in-plane disorder.

The stability of LBS beads and fluctuations of MOES beads [Figs. 3(b)–3(e)] show that the phase of the exciton density wave is locked at LBS defects and fluctuates in between them. Controlling the exciton density in the ring (by varying P and V) allows the fluctuations of the exciton density wave to be probed for different ratios between the MOES wavelength λ_c and the length L of the ring segment between two LBSs on the ring [such as LBS 1 and LBS 2 in Fig. 1(b)]. Figures 4(b) and 4(c) show that the amplitude of the fluctuations is small when the number of wavelengths of the exciton density wave confined between the defects $\nu = L/\lambda_c$ is an integer. In turn, fluctuations increase for noninteger ν; compare in Figs. 4(b) and 4(c) the middle panel presenting large fluctuations at noninteger ν with the left and right panels presenting smaller fluctuations at integer ν. Note that LBS bead positions are stable for any ν in adjacent ring segments, while MOES bead positions fluctuate. The large fluctuations of MOES bead positions shown in Figs. 3(b)–3(e) and the middle panel of Fig. 4 correspond to noninteger ν. However, at integer ν, fluctuations of MOES bead positions become almost as small as fluctuations of LBS bead positions [compare the left panel in Fig. 3(e) with the left and right panels in Fig. 4(c)].
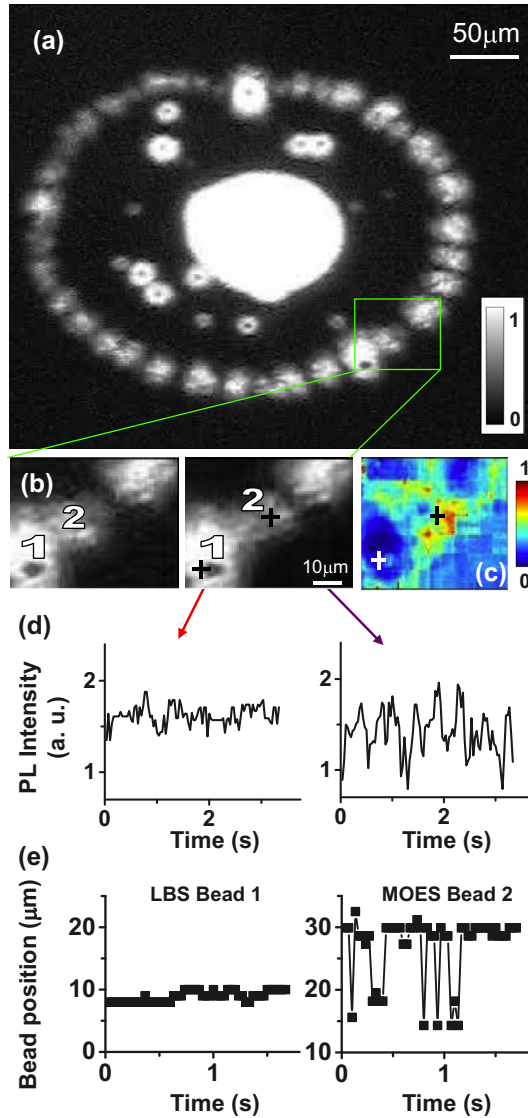
FIG. 3. (Color online) (a) IX emission pattern extracted from a real-time movie. (b) MOES bead positions fluctuate in time: left and right images are measured at the same parameters vs time. (c) Standard deviation of the IX emission intensity. Yellow (blue) color indicates high- (low-) fluctuation regions. (d) IX emission intensity vs time at the points marked by crosses in (b) and (c) around LBS bead (left) and MOES bead (right). (e) Bead position vs time for LBS bead (left) and MOES bead (right). $V = 1.217$ V.

This commensurability effect is quantified in Fig. 1(c), which presents the standard deviation $\sigma_{g^{(2)}}$ of the second-order correlation function $g^{(2)}(x) = \frac{\langle I(x')I(x'+x)\rangle}{\langle I(x')\rangle^2}$ for the IX emission intensity profile $I(x)$ along the exciton density wave between LBS 1 and LBS 2. Apparently, a stable periodic wave produces strong oscillations in the $g^{(2)}(x)$ correlation function with the distance between the maxima corresponding to the wave period, while fluctuations of the wave smear out such oscillations. Figure 1(a) shows that stronger oscillations in $g^{(2)}(x)$ are observed at integer ν. In turn, $\sigma_{g^{(2)}}$ gives a measure for the wave fluctuations: Large values of $\sigma_{g^{(2)}}$ correspond to a stable periodic wave, while small values of $\sigma_{g^{(2)}}$ correspond to stronger fluctuations which smear out the periodic wave
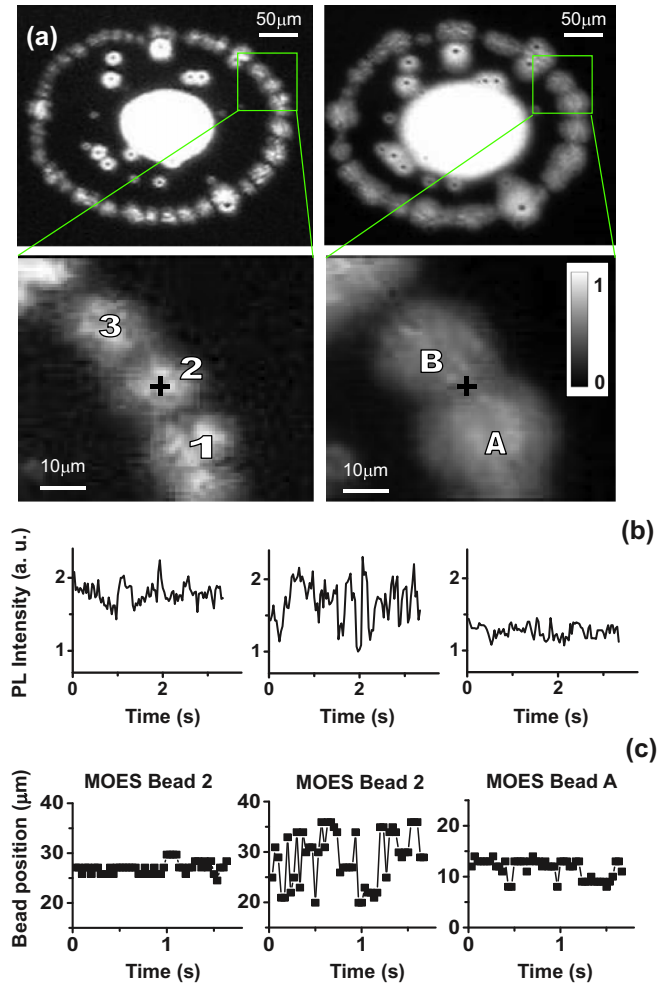

FIG. 4. (Color online) (a) Images of the IX emission pattern for different MOES wavelengths λ_c. The commensurability number $\nu = L/\lambda_c$ in the ring segment between LBS 1 and LBS 2 of length L is $\nu = 8$ (left) and 6 (right). (b) Fluctuations of the IX emission intensity for integer (left and right) and noninteger (middle) ν at the point marked by a cross in (a). (c) Fluctuations of the bead positions for the same conditions as in (b). $V = 1.219$ (left), 1.233 (middle), and 1.263 (right) V.

structure. Figure 1(c) shows pronounced maxima in $\sigma_{g^{(2)}}$, indicating suppression of the fluctuations of the exciton density wave at integer ν.

III. THEORY AND DISCUSSION

The MOES is a state with spontaneously broken symmetry involving a large number of excitons ($\sim 10^6$ in the ring segment between LBS 1 and LBS 2). The commensurability effect indicates that the fluctuations of the exciton density wave are collective. Collective fluctuation in states with spontaneously broken symmetry is a general phenomenon observed in a variety of both classical and quantum systems. Rotational fluctuations and waves in liquid crystals, sound waves in liquids and solids, and second-sound waves in superfluids present characteristic examples.

By developing a kinetic theory of the coupled electron-hole-exciton system, it has been shown that the transition into a spatially modulated state could be attributed to stimulated processes that build up near quantum degeneracy [22]. The stimulated processes provide the positive feedback for density fluctuation leading to spontaneous density modulation. This mechanism is consistent with the measured properties of the MOES outlined in the introduction: (i) the MOES is a condensate in momentum space [4–6], (ii) the MOES forms in the external ring on the interface between the electron-rich and hole-rich regions [29–33], and (iii) the MOES is characterized by repulsive IX interaction [20]. We note that the model [22] is a simplified model where negative feedback to density fluctuation, which is characteristic for both repulsive interaction and diffusion, is presented by diffusion, so the model qualitatively describes the underlying mechanism for the MOES formation. In Ref. [22] the effects of commensurability on the stability of the exciton density wave and their potential role in fluctuations were not addressed. Here, we make use of the same theoretical modeling scheme to gain insight into the commensurability effect described in Sec. II.

Following Ref. [22], the starting point of the analysis relies on a transport theory involving a system of coupled nonlinear diffusion equations for the electron, hole, and exciton densities, n_e, n_h, and n_x, with a local source for the holes, a distributed source for electrons, an electron-hole binding rate w, and an exciton recombination rate γ. In steady state, the solution of these transport equations predicts the development of a ring of exciton density separating a hole-rich region within the ring from an electron-rich region outside the ring. Further, by correlating w with n_x consistent with the effects of stimulated processes that build near quantum degeneracy, it was shown that when $u \equiv d \ln w / d \ln n_x \geqslant u_c$, there is a type-II instability towards the development of a symmetry-broken state in which the electron or hole and exciton densities acquire a periodic modulation around the ring.

To investigate the nature of the transition, the coupled transport theory can be approximated by an effective theory of the electron and exciton densities [22]. With a total carrier flux at the interface c and the diffusion length $\ell = (D_e D_h / cw)^{1/3}$, in the vicinity of the exciton ring, the dimensionless electron density, $g_e \equiv \frac{D_e}{c\ell} n_e$, satisfies the nonlinear diffusion equation

$$\dot{g}_e = \nabla^2 g_e - \exp\left[\frac{u}{\bar{g}_x(0)} \delta g_x\right] g_e(g_e - x), \qquad (1)$$

where lengths are measured in terms of the diffusion length ℓ, and fluctuation of the local exciton density from its value in the unmodulated steady state, $\delta g_x \equiv g_x - \bar{g}_x$, depends nonlocally on the fluctuation in electron density $\delta g_e \equiv g_e - \bar{g}_e$ through the relation

$$\delta g_x(\vec{x}) = -\delta g_e(\vec{x}) + \int \frac{\ell^2 d^2 x'}{2\pi \ell_x^2} K_0(|\vec{x} - \vec{x}'|\ell/\ell_x) \, \delta g_e(\vec{x}'),$$

with K_0 the modified Bessel function. In the limit of diverging c when the ring becomes infinite in size, u_c and λ_c depend parametrically and continuously on $\zeta = \ell/\ell_x$ [22].

To assess the potential for collective fluctuations to drive the observed commensurability effect, we investigated the influence of spatial confinement on the stability of the
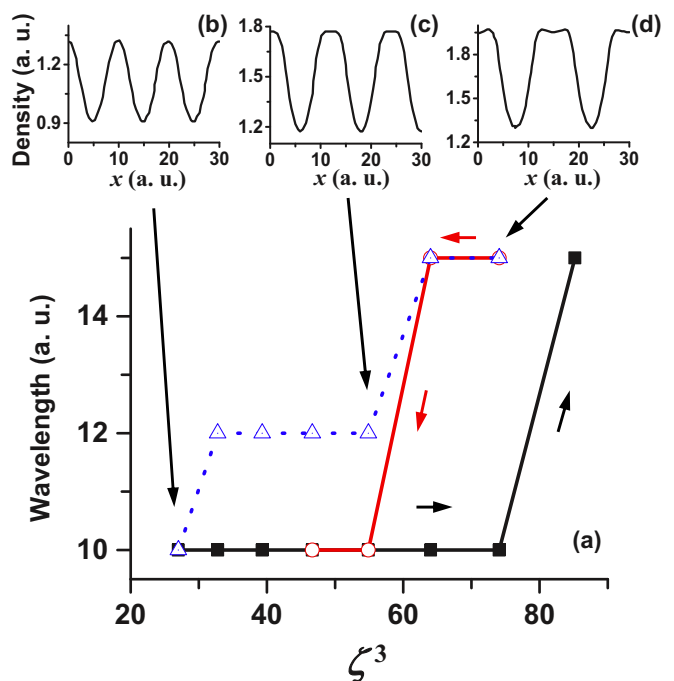

FIG. 5. (Color online) (a) Wavelength of the exciton density wave as a function of ζ^3 obtained from the numerical integration of the nonlinear transport equations (1). Squares (circles) show the evolution of λ_c as ζ is ramped up (down) progressively, using the previous state to define the seeding density. The triangles show the evolution of λ_c for a steady-state exciton density wave as ζ is ramped up using a small random perturbation from the uniform solution as an initial seeding density. (b)–(d) Corresponding profiles of the steady-state exciton density wave along the electron-hole interface. One-half of the total profile is shown so that the features are more visible on the panels. Commensurate states with integer $\nu = L/\lambda_c$ are found to be robust with respect to the parameter variation producing the plateaus, while fluctuations develop in the transition region between integer values of ν where hysteresis is found.

modulated state following continuous changes in the value of the control parameter ζ. Taking a fixed (but representative) value of $u/\bar{g}_x(0) = 10$, where the instability in the open system (i.e., where the ratio $\nu = L/\lambda_c$ of the ring circumference L to the wavelength of the modulation λ_c is large) is well developed, we first determined the steady-state profile of the spatial modulation of the exciton density as a function of changing ζ, allowing the steady state to develop from an initially radially symmetric (nonmodulated) state. For changing values of ζ, the steady-state configurations transit sequentially between configurations with integer values of ν. Taking the ring circumference to be $L = 60$ (in units of the diffusion length), the insets of Fig. 5 show the spatial profiles of the exciton density along the ring circumference at the electron-hole interface for three steady-state configurations (indexed by the blue triangles in the main figure).

To assess the stability of these configurations, we then considered the change of the steady state following an adiabatic change in ζ but now starting with the spatially modulated state as an initial configuration. In this case, one sees both hysteresis, with regions of the phase diagram in which the system remains trapped in a metastable state, and the exclusion of an

intermediate stable wave number [Fig. 5(a), red circles and black squares]. This behavior mirrors the commensurability effect seen in experiment—the stochastic transfer between stable and metastable states, a feature of discontinuous transitions, and the exclusion of stable modulations—a manifestation of the nonlinearity of the dynamics.

Within the model, the commensurability effect can be qualitatively understood as follows: When the natural wavelength of the instability translates to an integer ν the wavelength in the constrained ring geometry does not change within large variations in ζ, indicating that the exciton density wave is stable against fluctuations. However, when the natural wavelength translates to noninteger ν the wavelength changes dramatically with small variations in ζ, indicating that the exciton density wave is unstable.

Finally, the observed enhancement of both the MOES wavelength λ_c and the ring width δ_r with density [Fig. 2(c)] is also consistent with the model. Indeed, within the model $\lambda_c \sim (\ell_x/\ell)^{2/3}\ell$ and $\delta_r \sim \ell_x$ and both increase with density as ℓ_x and ℓ increase with density due to screening of the in-plane disorder.

The commensurability effect shows that the MOES is a collective phenomenon. Earlier measurements revealed that the coherence length in the MOES is an order of magnitude greater than in a classical exciton gas, identifying MOES as a quantum bosonic gas [4–6]. However, the coherence length in the MOES is limited to a few micrometers and is significantly smaller than the MOES wavelength [$\lambda_c \sim$

few tens of micrometers; see Fig. 2(c)]. In contrast, the commensurability effect presents collective behavior of the entire macroscopic system of excitons in the ring segment of length ~ 100 μm containing several MOES wavelengths [Fig. 1(b)]. This shows that the commensurability effect is a collective phenomenon in quantum bosonic gases.

The studies of fluctuation and commensurability effects can be extended to various geometries, which can be arranged by positioning the ring relative to different LBSs and also relative to various in-plane potential landscapes created and controlled by lateral voltage patterns. For an overview of controllable in-plane potential landscapes for IXs, see Ref. [38] and references therein.

IV. SUMMARY

We observed fluctuations of the exciton density wave and the commensurability effect—the fluctuation suppression when the number of wavelengths confined between defects is an integer.

ACKNOWLEDGMENTS

[1] Yu. E. Lozovik and V. I. Yudson, J. Exp. Theor. Phys. **44**, 389 (1976).

[2] T. Fukuzawa, S. S. Kano, T. K. Gustafson, and T. Ogawa, Surf. Sci. **228**, 482 (1990).

[3] L. V. Butov, A. C. Gossard, and D. S. Chemla, Nature (London) **418**, 751 (2002).

[4] M. Alloing, M. Beian, M. Lewenstein, D. Fuster, Y. González, L. González, R. Combescot, M. Combescot, and F. Dubin, Europhys. Lett. **107**, 10012 (2014).

[5] Sen Yang, A. T. Hammack, M. M. Fogler, L. V. Butov, and A. C. Gossard, Phys. Rev. Lett. **97**, 187402 (2006).

[6] A. A. High, J. R. Leonard, A. T. Hammack, M. M. Fogler, L. V. Butov, A. V. Kavokin, K. L. Campman, and A. C. Gossard, Nature (London) **483**, 584 (2012).

[7] D. Nandi, A. D. K. Finck, J. P. Eisenstein, L. N. Pfeiffer, and K. W. West, Nature (London) **488**, 481 (2012).

[8] A. A. High, A. T. Hammack, J. R. Leonard, Sen Yang, L. V. Butov, T. Ostatnický, M. Vladimirova, A. V. Kavokin, T. C. H. Liew, K. L. Campman, and A. C. Gossard, Phys. Rev. Lett. **110**, 246403 (2013).

[9] L. V. Butov and A. I. Filin, Phys. Rev. B **58**, 1980 (1998).

[10] I. B. Spielman, J. P. Eisenstein, L. N. Pfeiffer, and K. W. West, Phys. Rev. Lett. **84**, 5808 (2000).

[11] J. P. Eisenstein and A. H. MacDonald, Nature (London) **432**, 691 (2004).

[12] L. V. Butov, A. L. Ivanov, A. Imamoglu, P. B. Littlewood, A. A. Shashkin, V. T. Dolgopolov, K. L. Campman, and A. C. Gossard, Phys. Rev. Lett. **86**, 5608 (2001).

[13] B. Karmakar, V. Pellegrini, A. Pinczuk, L. N. Pfeiffer, and K. W. West, Phys. Rev. Lett. **102**, 036802 (2009).

[14] M. Remeika, J. C. Graves, A. T. Hammack, A. D. Meyertholen, M. M. Fogler, L. V. Butov, M. Hanson, and A. C. Gossard, Phys. Rev. Lett. **102**, 186803 (2009).

[15] A. V. Gorbunov and V. B. Timofeev, JETP Lett. **96**, 138 (2012).

[16] A. V. Gorbunov and V. B. Timofeev, Solid State Commun. **157**, 6 (2013).

[17] G. J. Schinner, J. Repp, E. Schubert, A. K. Rai, D. Reuter, A. D. Wieck, A. O. Govorov, A. W. Holleitner, and J. P. Kotthaus, Phys. Rev. B **87**, 205302 (2013).

[18] Y. Shilo, K. Cohen, B. Laikhtman, K. West, L. Pfeiffer, and R. Rapaport, Nat. Commun. **4**, 2335 (2013).

[19] M. Stern, V. Umansky, and I. Bar-Joseph, Science **343**, 55 (2014).

[20] Sen Yang, A. V. Mintsev, A. T. Hammack, L. V. Butov, and A. C. Gossard, Phys. Rev. B **75**, 033311 (2007).

[21] S. R. E. Yang, Q. H. Park, and J. Yeo, Int. J. Mod. Phys. B **18**, 3797 (2004).

[22] L. S. Levitov, B. D. Simons, and L. V. Butov, Phys. Rev. Lett. **94**, 176404 (2005).

[23] A. A. Chernyuk and V. I. Sugakov, Phys. Rev. B **74**, 085303 (2006).

[24] A. V. Paraskevov and T. V. Khabarova, Phys. Lett. A **368**, 151 (2007).

[25] C. S. Liu, H. G. Luo, and W. C. Wu, Phys. Rev. B **80**, 125317 (2009).

[26] J. Wilkes, E. A. Muljarov, and A. L. Ivanov, Phys. Rev. Lett. **109**, 187402 (2012).

[27] S. V. Andreev, Phys. Rev. Lett. **110**, 146401 (2013).

[28] S. V. Andreev, A. A. Varlamov, and A. V. Kavokin, Phys. Rev. Lett. **112**, 036401 (2014).

[29] L. V. Butov, L. S. Levitov, A. V. Mintsev, B. D. Simons, A. C. Gossard, and D. S. Chemla, Phys. Rev. Lett. **92**, 117404 (2004).

[30] R. Rapaport, G. Chen, D. Snoke, S. H. Simon, L. Pfeiffer, K. West, Y. Liu, and S. Denev, Phys. Rev. Lett. **92**, 117405 (2004).

[31] G. Chen, R. Rapaport, S. H. Simon, L. Pfeiffer, and K. West, Phys. Rev. B **71**, 041301(R) (2005).

[32] M. Haque, Phys. Rev. E **73**, 066207 (2006).

[33] Sen Yang, L. V. Butov, L. S. Levitov, B. D. Simons, and A. C. Gossard, Phys. Rev. B **81**, 115320 (2010).

[34] A. L. Ivanov, L. E. Smallwood, A. T. Hammack, Sen Yang, L. V. Butov, and A. C. Gossard, Europhys. Lett. **73**, 920 (2006).

[35] M. Remeika, A. T. Hammack, S. V. Poltavtsev, L. V. Butov, J. Wilkes, A. L. Ivanov, K. L. Campman, M. Hanson, and A. C. Gossard, Phys. Rev. B **88**, 125307 (2013).

[36] D. Yoshioka and A. H. MacDonald, J. Phys. Soc. Jpn. **59**, 4211 (1990).

[37] See Supplemental Material at http://link.aps.org/supplemental/10.1103/PhysRevB.91.245302 for a real-time movie of the IX emission pattern. It shows that LBS beads are stable while MOES beads fluctuate with time.

[38] M. Remeika, M. M. Fogler, L. V. Butov, M. Hanson, and A. C. Gossard, Appl. Phys. Lett. **100**, 061103 (2012).